Engineered calmodulins reveal the unexpected eminence of Ca^{2+} channel inactivation in controlling heart excitation

Badr A. Alseikhan, Carla D. DeMaria, Henry M. Colecraft, and David T. Yue*

Calcium Signals Laboratory, Program in Molecular and Cellular Systems Physiology, Departments of Biomedical Engineering and Neuroscience, The Johns Hopkins University School of Medicine, Ross Building, Room 713, 720 Rutland Avenue, Baltimore, MD 21205

Edited by Harald Reuter, University of Bern, Bern, Switzerland, and approved October 23, 2002 (received for review June 21, 2002)

Engineered calmodulins (CaMs), rendered Ca^{2+}-insensitive by mutations, function as dominant negatives in heterologous systems, and have revealed mechanisms of ion channel modulation by Ca^{2+}/CaM. The use of these CaMs in native mammalian cells now emerges as a strategy to unmask the biology of such Ca^{2+} feedback. Here, we developed recombinant adenoviruses bearing engineered CaMs to facilitate their expression in adult heart cells, where Ca^{2+} regulation may be essential for moment-to-moment control of the heartbeat. Engineered CaMs not only eliminated the Ca^{2+}-dependent inactivation of native calcium channels, but exposed an unexpectedly large impact of removing such feedback: the unprecedented (4- to 5-fold) prolongation of action potentials. This striking result recasts the basic paradigm for action-potential control and illustrates the promise of virally delivered engineered CaM to investigate the biology of numerous other CaM-signaling pathways.

An intriguing capability of calmodulin (CaM) is that even its Ca^{2+}-free form (apoCaM) may preassociate with certain target molecules, whose function is subsequently modulated when an elevation of Ca^{2+} calcifies the associated CaM, and the resulting Ca^{2+}/CaM shifts to a different site on the target (1). This configuration endows CaM-driven modulation with selective responsiveness to local Ca^{2+} activity near the regulated molecule (2). By contrast, the original view of CaM, still pertinent to other molecules, holds that only on calcification does CaM diffuse and bind to a target (3), such that CaM-mediated regulation responds to global Ca^{2+}.

Despite the enormous potential biological implications of Ca^{2+} signaling by preassociated CaM, its prevalence and functional ramifications remain poorly resolved, because establishing an apoCaM/target association by *in vitro* biochemistry can be especially challenging (1), and the pharmacological inhibition of preassociated CaM may be precluded by steric protection within an apoCaM/target complex (4–7). A recently developed approach, in the discovery of ion-channel regulation by preassociated CaM, involves coexpression of recombinant channels and engineered CaM in heterologous expression systems. The engineered CaM, rendered Ca^{2+}-insensitive by point mutations (8), preassociates with coexpressed channels (9), blocks endogenous CaM from accessing Ca^{2+}/CaM effector sites, and thus eliminates Ca^{2+} regulation of those channels. This strategy has revealed a role for preassociated CaM in the regulation of small-conductance K channels (7), L-type Ca^{2+} channels (8, 10), P/Q-type Ca^{2+} channels (2), and store-operated channels (11). Given this success, we wondered whether the acute expression of engineered CaMs in native mammalian cells could engage a higher-order challenge: defining the *in situ* biological impact of Ca^{2+} feedback involving preassociated CaM.

As an important test of this tactic, we used virus-mediated expression of engineered CaM in adult heart cells to explore the physiological role of Ca^{2+}-dependent inactivation (CDI) of cardiac L-type Ca^{2+} channels, a process involving preassociated CaM (8–10). CDI of L-type channels and activation of numerous K channels are believed to control cardiac action-potential duration (APD) (12), a vital excitability parameter whose prolongation in heart failure (13) and long QT syndromes (12) precipitates life-threatening arrhythmias (14). The inability to selectively eliminate CDI in heart cells has proven to be a critical impediment to resolving the relative roles of the diverse channels in controlling APD. Overexpression of engineered CaM in heart cells could remove this restrictive limitation, and directly define the impact of L-type channel CDI on the cardiac action potential.

Materials and Methods

Adenoviral vector construction, rat and guinea pig heart cell isolation, and viral transduction were done as described (15). CaM protein was quantitated by Western blot analysis (9). Whole-cell calcium currents were recorded under voltage clamp (8, 15) in the presence of 0.5 μmol/liter ryanodine in bath solution. Action potentials were recorded as described (13). APD was measured as the duration between upstroke and repolarizing crossings at -32.5 mV. Cells were studied irrespective of GFP fluorescence, except for AdIR-CaM_{1234} experiments in Fig. 3 *D* and *E*. All average electrophysiology data are presented as mean $\pm$ SEM, after analysis by custom software in MATLAB (Mathworks, Natick, MA). Differences were considered statistically significant at $P < 0.05$, and ANOVA/Bonferroni analysis was applied to APD comparisons in Fig. 3 (see *Supporting Materials and Methods*, which is published as supporting information on the PNAS web site, www.pnas.org).

Results

Development of Recombinant Adenoviruses Bearing Engineered CaMs. To use engineered Ca^{2+}-insensitive CaM for investigation of CaM biology, it is necessary to achieve severalfold overexpression of engineered vs. endogenous CaM, thereby enriching molecular preassociation sites with recombinant CaM (9). Given the notorious difficulty of using conventional nonviral methods to introduce exogenous DNA into cardiac myocytes (16) and other terminally differentiated native cells, we created recombinant adenoviruses bearing wild-type or various mutant Ca^{2+}-insensitive CaMs (8), all driven constitutively by a strong cytomegalovirus promoter. Such adenoviruses, renowned for their high-efficiency transduction capacity in heart cells (17), promised to produce the requisite expression levels of engineered CaM. A critical virus-creation strategy was to exploit the high-efficiency, enzyme-driven recombination of CaM and viral genes, according to a Cre-Lox/Cre-recombinase system (18, 19). This approach permitted stringent selection for CaM-containing over wild-type adenovirus, a strategic consideration when the

This paper was submitted directly (Track II) to the PNAS office.

Abbreviations: CaM, calmodulin; CDI, Ca^{2+}-dependent inactivation; APD, action-potential duration.

*To whom correspondence should be addressed. E-mail: dyue@bme.jhu.edu.

incorporation of Ca^{2+}-insensitive CaM may entail a negative-selection bias. Another important feature was to enfold engineered CaM within the context of a bicistronic construct, where an internal ribosome entry site (IRES) motif was sandwiched between the genes for CaM and GFP (20). This construct would then direct expression of engineered CaM and GFP as separate polypeptides, thus identifying infected myocytes by fluorescence without any functional perturbation of CaM induced by its fusion to GFP.

Baseline characterization of CaM-bearing adenovirus in adult rat ventricular myocytes revealed robust expression of engineered CaM (AdIR-CaM) without an appreciable nonspecific perturbation of cell properties (Fig. 1). From populations of virally transduced myocytes, Western blot analysis of recombinant CaM proteins (Fig. 1*A*) confirmed strong overexpression (>10-fold) of all recombinant CaM forms relative to endogenous CaM. At the level of individual cells, control myocytes, cultured for 48 h, retained the regular striations and rod-shaped morphology characteristic of native heart cells (Fig. 1*B Left*). Transduced myocytes, cultured identically but treated with virus bearing wild-type CaM (AdIR-CaM_{WT}), showed little morphological change from controls, but were readily distinguished by green fluorescence present in 50–100% of cells, depending on viral titer (Fig. 1*B Right*). From the perspective of L-type Ca^{2+} channels in single cells, treatment with AdIR-CaM_{WT} was also devoid of untoward nonspecific effects. Fig. 1*C* summarizes channel behavior in control uninfected cells, where there was clearly a faster decay of Ca^{2+} vs. Ba^{2+} current (Fig. 1*C Top*), owing to CaM-driven CDI (8). On average, the fraction of Ca^{2+} current remaining after depolarizing for 100 ms (r_{100}) exhibited a deep U-shaped voltage dependence (Fig. 1*C Middle*), characteristic of genuine CDI. By contrast, the Ba^{2+} r_{100} relation demonstrated a shallower, monotonic decline with increasing depolarization, consistent with a slower voltage-dependent inactivation process (5). The difference between the two relations at +10 mV ($f \sim 0.3$) thus provided a convenient measure of pure CDI (8). These inactivation characteristics, along with the bell-shaped current–voltage relation (Fig. 1*C Bottom*) reflecting channel activation, were typical for rat heart cells (5). In cells treated with AdIR-CaM_{WT}, both CDI and the voltage-dependence of activation were reassuringly indistinguishable (Fig. 1*D*), arguing that endogenous CaM was not a limiting factor in native L-type channel function. Altogether, the close similarity of cell morphology and L-type channel properties between control and treated cells discounted the spurious effects of adenoviral treatment, enabling subsequent testing for specific effects of overexpressing engineered CaMs.

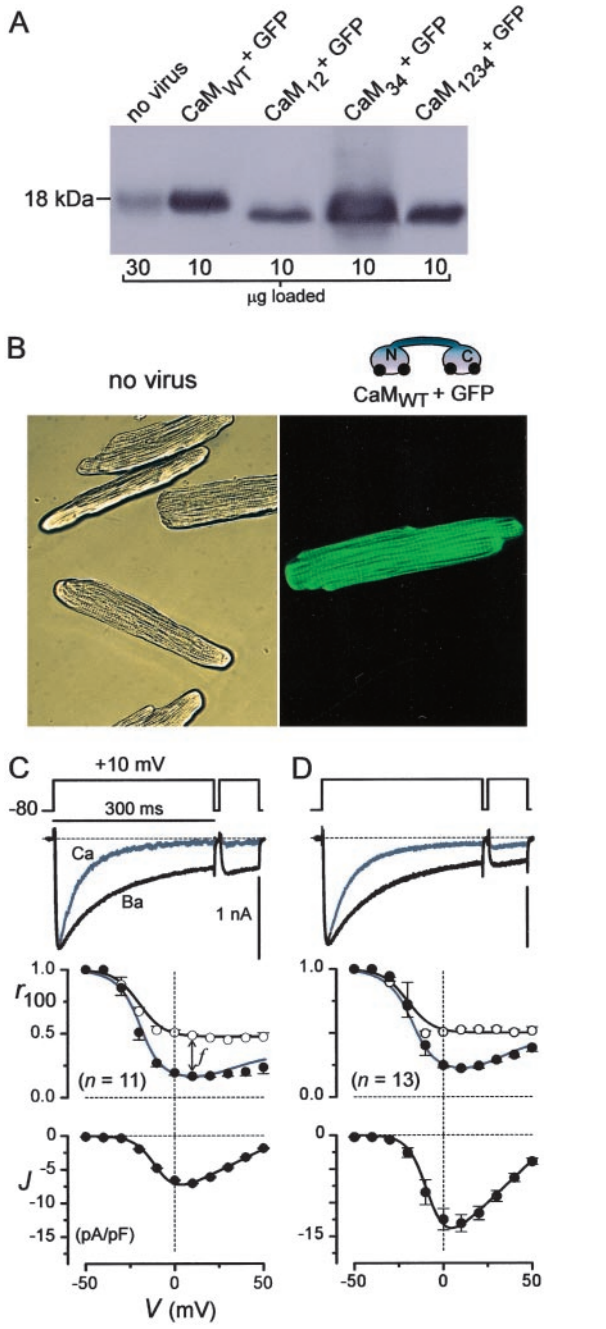

Fig. 1. Delivery of engineered CaMs to myocytes. (*A*) CaM Western blots from rat cardiocytes (9), cultured for 2 d after infection. Lysate amount per lane is indicated at the bottom. (*B*) Micrographs (×400) relating to *A*, with uninfected cells in bright-field (*Left*) and cells with AdIR-CaM under fluorescence (*Right*). (*C* and *D*) L-type channels in cells relating to those in *B*. (*Top*) Exemplar currents with Ca^{2+} (gray) or Ba^{2+} (black) as the charge carrier. The Ca^{2+} trace was amplified ≈×3 to match the Ba^{2+} traces; scale bars for Ba^{2+}. (*Middle*) Mean CDI properties shown by Ca^{2+} and Ba^{2+} r_{100} curves, and the average of *n* cells. *f* is defined at +10 mV. ○, Ba^{2+}; ●, Ca^{2+}. (*Bottom*) Peak current density, with Ca^{2+}, the mean from the same *n* cells. GFP inexplicably enhanced the current.

Engineered CaMs Eliminate L-Type Channel CDI in Heart Cells. In heterologous systems, overexpression of CaM_{1234}, a Ca^{2+}-insensitive CaM mutant harboring aspartate-to-alanine mutations in all four EF hands (8) (Fig. 2*A Top*), clearly eliminates the CDI of recombinant L-type channels translated concurrently with engineered CaM (8). However, for this dominant-negative action to occur in native cells like myocytes, engineered CaM_{1234} must exchange sufficiently with wild-type endogenous CaM, which would be bound to preexisting native L-type channels. It has, therefore, been uncertain as to whether overexpression of molecules like CaM_{1234} could, in general, eliminate CaM signaling in native cells, as would be required for engineered CaMs to dissect CaM biology *in vivo*.

Given the relative abundance of L-type Ca^{2+} channels in rat ventricular myocytes (21), determining the impact of overexpressing CaM_{1234} on their Ca^{2+} currents provided a rather stringent test of engineered CaM to displace its endogenous counterpart. Exemplar traces from one such cell demonstrated complete elimination of CDI (Fig. 2*A Top*), suggesting robust displacement of endogenous CaM. Population data (Fig. 2*D*) indicated a strong ≈60% inhibition of CDI, as determined from cells investigated irrespective of GFP fluorescence to gauge mean impact over the entire culture. We further tested whether CaM_{1234} exerted selective effects on CDI by pursuing in-depth biophysical analysis in cells manifesting the strongest attenuation

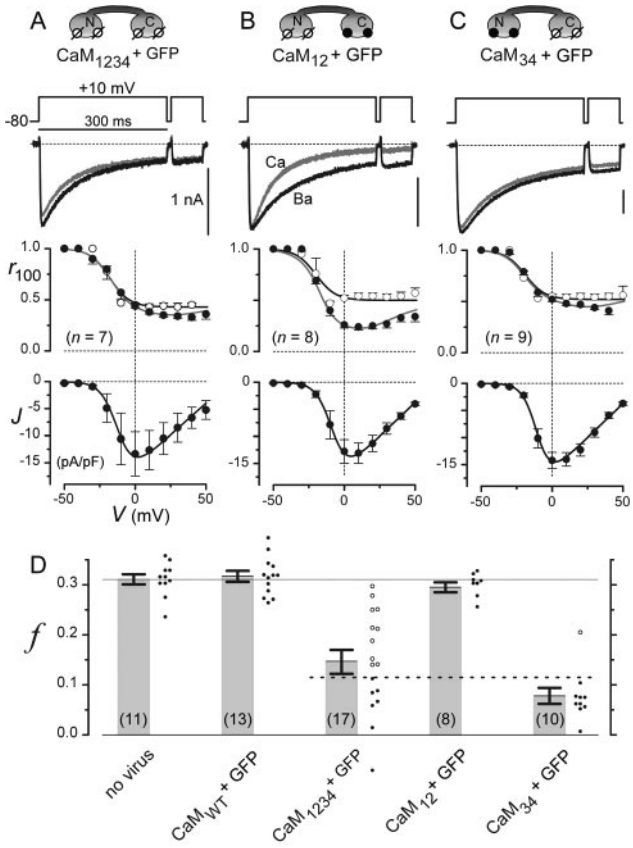

Fig. 2. Engineered CaMs eliminate native L-type channel CDI. (*A–C*) L-type channel properties in rat cells with engineered CaMs, drawn at the top. The format used here is the same as in Fig. 1*C*. The means are from cells relating to solid circles in *D*. ○, Ba^{2+}; ●, Ca^{2+}. (*D*) The bars show population CDI properties, reflected by *f* (see Fig. 1*C*). Associated cell-by-cell scattergram are shown. Dotted line, *f* cutoff for inclusion in the means of *A* and *C*. The left two bars relate to Fig. 1 *C* and *D*.

of CDI, as defined by $f < 0.12$ (Fig. 2*D*, solid symbols below dashed line). For this select subset of cells, Ca^{2+} and Ba^{2+} r_{100} curves (Fig. 2*A Middle*) were virtually superimposable and no different from the Ba^{2+} r_{100} curve of uninfected cells (Fig. 1*C*). CDI was therefore eliminated without change in the voltage-dependent inactivation present with Ba^{2+}. Moreover, the voltage dependence of activation (Fig. 2*A Bottom*) was no different from that of controls (Fig. 1*C*). These results demonstrated that CaM_{1234} can efficiently displace endogenous CaM on native L-type channels, resulting in strong inhibition of CDI without perturbation of other gating functions.

Additional selectivity of CaM action might be obtained if native L-type channel CDI was exclusively reliant on Ca^{2+} signaling through the C-terminal lobe of CaM, as demonstrated thus far in heterologous channel expression experiments (8). Enhanced selectivity of engineered CaM might then be achieved by restricting aspartate-to-alanine mutations described for CaM_{1234} to the C-terminal lobe (8) (Fig. 2*C Top*, CaM_{34}), thus preserving CaM signaling to molecular targets reliant on Ca^{2+} binding to the N-terminal lobe (22). Alternatively, restricting mutations to the N-terminal lobe (8) (Fig. 2*B Top*, CaM_{12}) would engage CaM biology related to the latter class of targets, while preserving signaling to molecules like the L-type channel. Fig. 2 *B–D* demonstrates that such CaM lobe-specific signaling to native L-type channels is indeed recapitulated in heart cells. Transduction of cells by AdIR-CaM_{12} completely spares control channel behavior (Fig. 2 *B* and *D*), whereas AdIR-CaM_{34} functions just as AdIR-CaM_{1234} to selectively eliminate CDI (Fig. 2 *C* and *D*).

Overall, the results in Fig. 2 demonstrated therefore that viral delivery of engineered CaMs can rather selectively eliminate the CDI of native L-type channels, thus providing a promising opportunity to investigate the biological impact of eliminating this Ca^{2+} feedback process. In particular, an emerging view presumes that a delicate balance, between the waxing of activating K channels and the waning of inactivating L-type Ca^{2+} channels, specifies cardiac APD (12). This duration is critically important because disturbance of its control spawns life-threatening cardiac dysrhythmias (12). Here, then, viral delivery of engineered CaM promised a direct determination of the relative importance of L-type channel CDI in maintaining this vital balance.

Elimination of CDI Produces "Ultralong" Action Potentials. To assess the impact of L-type channel CDI on cardiac action potentials, we turned to guinea pig ventricular myocytes, because of the great similarity and relevance of their action potentials to those of humans. Untransduced myocytes, cultured for 24 h, exhibited unremarkable action potentials, as demonstrated by exemplar waveforms (Fig. 3*A*, NV) and mean durations of ≈400 ms (Fig. 3*B*, APD = 387 ± 50 ms). In transduced myocytes, cultured identically but exposed to AdIR-CaM_{WT}, action potentials were no different from control (Fig. 3 *A* and *B*, WT; APD = 420 ± 58 ms), fitting with unchanged gating of L-type channels during CaM_{WT} overexpression (Fig. 1*D*). In striking contrast, overexpression of CaM_{1234} produced an unexpectedly profound, 4- to 5-fold prolongation of APD (Fig. 3 *A* and *B*, 1234; APD = 1821 ± 243 ms), mainly stemming from the lengthening of the plateau phase without appreciable change in other waveform characteristics. Such "ultralong" action potentials rank among the most enduring reported in the literature, far exceeding those in heart failure (13) or transgenic knockouts of K channels (23). Our results, thus, appeared inconsistent with prevailing assumptions about the codominance of K channel activation and Ca^{2+} channel inactivation in controlling APD (12), and instead pointed to a preeminence of Ca^{2+} channel CDI in setting this essential excitability parameter.

Because engineered CaM could also affect molecules other than L-type channels, it was critical to test whether the action-potential prolongation could be linked selectively to the elimination of CDI. First, we confirmed that L-type channel CDI was attenuated in guinea pig myocytes exposed to AdIR-CaM_{1234}, and cultured for 24 h as in action-potential experiments. In fact, fitting with the lower density of L-type channels in guinea pig (21), elimination of CDI was even stronger than in rat, and nearly completely irrespective of GFP fluorescence (Fig. 3*C*, $f \approx 0$ with CaM_{1234}). Second, the CaM lobe-specificity of action-potential prolongation fit precisely with that of L-type channel CDI. Treatment with AdIR-CaM_{12} left action potentials the same as that of controls (Fig. 3 *A* and *B*, 12; APD = 336 ± 44 ms), and AdIR-CaM_{34} induced ultralong action potentials (Fig. 3*A*, 34; APD = 1546 ± 173 ms) identical to those observed with AdIR-CaM_{1234} (Fig. 3*B*, 34 vs. 1234). The difference in exemplar traces for CaM_{34} and CaM_{1234} (Fig. 3*A*) simply illustrates the range of behavior within either group. Third, K channel currents, the other major set of ion fluxes believed to strongly impact APD, were unchanged by exposure to AdIR-CaM_{1234} (Fig. 3*D*). Exemplar traces (Fig. 3*D Top*), drawn from untransduced and AdIR-CaM_{1234} cells, showed closely similar kinetics and amplitudes of K current. Inward currents reflect inward rectifier (I_{K1}) K channels, and outward currents represent a composite of transient outward (24) (I_{to}) and delayed rectifier (I_{Kr}, I_{Ks}) K channels (25). Population data completely confirmed the similarity, as mean inward and outward K current densities (Fig. 3*D Bottom*) were indistinguishable between the two groups of cells.

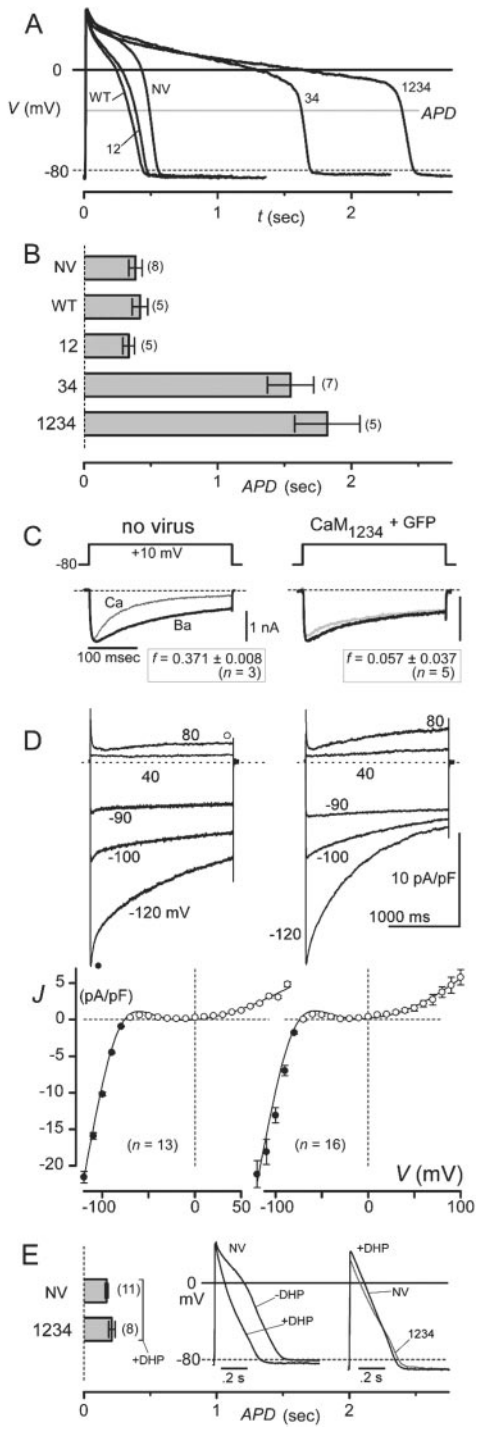

Fig. 3. Ultralong action potentials in guinea pig myocytes lacking CDI. (*A*) Exemplar action potentials (APs) in uninfected cells (NV), and in cells with AdIR-CaMs (WT, CaM_{WT}+GFP; 12, CaM_{12}+GFP; 34, CaM_{34}+GFP; 1234, CaM_{1234}+GFP). Gray line, voltage for APD (*APD*) measurement. Waveform differences for WT, 12, and NV illustrate variability observable within any one of groups; group means are statistically indistinguishable in *B*. Likewise, 34 and 1234 exemplars illustrate variability present in either group; there is no statistical difference of groups means in *B*. (*B*) Mean APDs, from populations relating to exemplars in *A*. APDs for NV, WT, and 12 were statistically indistinguishable, as were those for 34 and 1234. APD differences between these two groups were significant. (*C*) Engineered CaMs eliminate CDI in guinea pig cells. Exemplar L-type currents from uninfected cells (*Left*), and those with AdIR-CaM_{1234} (*Right*); format is as in Fig. 1*C Top*. Mean *f* below indicates approximately complete elimination of CDI by CaM_{1234}. (*D*) No K current change by engineered CaMs in guinea pig cells. (*Left*), Uninfected cells. (*Right*) Cells with AdIR-CaM_{1234}. (*Upper*) Exemplar K currents during steps to marked voltages, from −70 mV holding potential. (*Lower*) K current-voltage curves, averaged from *n* cells in each population. ●, Peak K currents at voltage-pulse onset; ○, K currents at end of 2-s pulses. (*E*) No APD prolongation by CaM_{1234} with nimodipine (10 μM). Bar graph, format as in *B*; APDs with nimodipine are significantly shorter than counterparts in *B*; there is no statistical difference between NV and 1234 in *E*. (*Left Inset*) AP in NV exemplar cell, ±nimodipine (±DHP). (*Right Inset*), exemplar NV and 1234 (gray) APs with nimodipine.

Finally, to investigate whether CaM_{1234} effects on still other determinants of excitability contributed to the ultralong responses, we examined action potentials during selective pharmacological blockade of L-type Ca^{2+} current (Fig. 3*E*). Elimination of L-type current normally yields abbreviated action potentials sustained by all remaining ion transport mechanisms (26), and spares a portion of Ca^{2+} cycling driven by sodium–calcium exchange (27). Under these conditions, CaM_{1234} would prolong action potentials only if there were pertinent effects on transport mechanisms other than L-type channels. The clear absence of such prolongation (Fig. 3*E*) strongly argues against such a possibility, leaving elimination of L-type channel CDI as the predominant causative factor underlying our ultralong action potentials (Fig. 3 *A* and *B*). This conclusion might also have been anticipated by considering the potential scope of CaM effects on other transport mechanisms. In some instances, a small fraction of slowly inactivating Na channels could prolong action potentials (28); however, CaM_{1234} would, if anything, diminish the prevalence of slow inactivation (29, 30). CaM may preassociate with cardiac ryanodine receptor channels (31) situated on intracellular stores of Ca^{2+}, but preliminary evidence in live cells suggests that CaM_{1234} would, if anything, promote Ca^{2+} release† and thereby CDI. More importantly, complete pharmacological elimination of phasic Ca^{2+} release through ryanodine receptors has, at most, small effects on APD (33). The effects of eliminating L-type channel CDI on APD could be amplified by sodium–calcium exchange (34); long-lasting Ca^{2+} influx through L-type channels may potentiate inward exchange current through positive shifts in exchanger reversal potential and Ca^{2+}-induced allosteric facilitation (35). However, it is unlikely that CaM_{1234} acts directly through sodium-calcium exchanger to produce the ultralong responses, because Ca^{2+} binding to the exchanger itself probably initiates allosteric facilitation (36). Furthermore, if CaM were to contribute to facilitation, CaM_{1234} would presumably inhibit inward exchanger current, thereby shortening action potentials.

Discussion

Experiments with viral delivery of engineered CaMs have revealed an unexpected dominance of the CDI of L-type Ca^{2+} channels in controlling the duration of cardiac action potentials. Given the undisputed importance of K currents in the genesis of the action-potential plateau phase (12, 14), how does this preeminence of L-type channel CDI come about?

Clear answers to this paradox come from the adaptation of an elegant graphical analysis for predicting key action-potential landmarks (37, 38). In particular, this approach succinctly articulates the disposition of ionic fluxes that causes transition from plateau to repolarizing phase of the action potential (Fig. 4*A*, *e*). The crux of the analysis is to consolidate all surface-membrane ionic flux during the plateau phase in terms of a single, quasi-instantaneous current–voltage relation. In essence, this relationship approximates the total cellular current at a given membrane potential, if one waits a few ms before viewing current after a

†Sobie, E., Alseikhan, B. A., Colecraft, H. M., Yue, D. T. & Lederer, W. J. (2001) *Biophys. J.* **80,** 508a (abstr.).

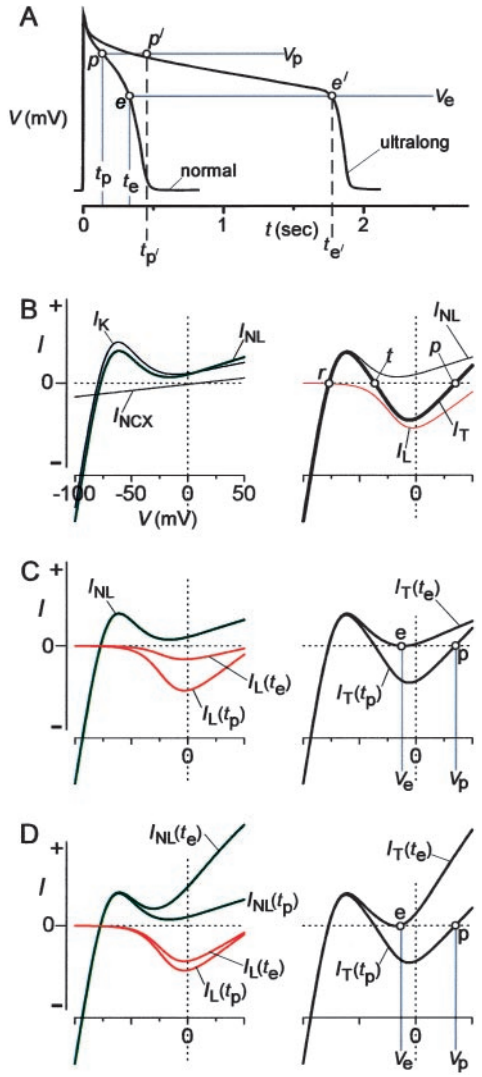

Fig. 4. Graph I_T analysis implicates CDI as dominant APD control factor. (*A*) Schematic of prototypic ''normal'' and ''ultralong'' action potentials (APs). Labeled time, voltage, and waveform landmarks relate to analysis in *B–D*. (*B*) Formulation of I_T analysis. (*Left*) Aggregate current–voltage relation for non-L-type current (I_{NL}), equal to sum of curves for K channels (I_K) and Na/Ca exchanger (I_{NCX}). All relations here and throughout the figure are schematized for conceptual clarity. (*Right*) Aggregate current–voltage relation for entire cell (I_T), equal to sum of I_{NL} (from left) and L-type channel (I_L) relations. I_T zero-crossing points predict resting potential (*r*), threshold potential (*t*), and plateau of action potential (*p*). (*C*) Dominant (L-type channel) CDI case. (*Left*) Main time-dependent change during latter plateau of normal AP is CDI, yielding a smaller $I_L(t_e)$ than $I_L(t_p)$, and invariant I_{NL}. (*Right*) Summing $I_L(t_p)$ and I_{NL} yields $I_T(t_p)$, relating to normal AP plateau in *A*. Adding $I_L(t_e)$ and I_{NL} yields $I_T(t_e)$, signaling termination of normal AP in *A* (point *e*). (*D*) Dominant K activation scenario. (*Left*) Main time-dependent change during latter plateau is K channel activation, yielding much larger $I_{NL}(t_e)$ than $I_{NL}(t_p)$, and slight decrease of $I_L(t_e)$ vs. $I_L(t_p)$. (*Right*) Summing $I_L(t_p)$ and $I_{NL}(t_p)$ produces $I_T(t_p)$, predicting normal AP plateau in *A*. Adding $I_L(t_e)$ and $I_{NL}(t_e)$ produces $I_T(t_e)$, precipitating termination of plateau in *A* (point *e*).

change in voltage. To form such a relationship, we first consider the status of K currents by the mid-plateau phase (>200 ms after depolarization), as apparent in our K current records (Fig. 3*D*). Transient outward K channels would be fully inactivated (24), delayed rectifier K channel opening (I_{Kr}, I_{Ks}) would change very slowly with time, and inward rectifier current would be defined by its instantaneous current–voltage relationship (39). Hence, aggregate K current can be specified by a quasi-instantaneous relation summed from the individual instantaneous current–voltage relations of inward and delayed rectifier currents (Fig. 4*B Left*, I_K). Regarding sodium–calcium exchange, reversal potential and allosteric facilitation would also be changing slowly by this point in the action potential (34), hence, the instantaneous relation for this exchanger serves as its quasi-instantaneous function (Fig. 4*B Left*, I_{NCX}). Together, the quasi-instantaneous relations I_K and I_{NCX} can be combined into a single I_{NL} relation (Fig. 4*B Left*). Because Na channels would be inactivated by the midplateau phase, the only remaining current would flow through L-type channels. Over the time course of a few milliseconds, activation gating of this channel would equilibrate rapidly with changes in voltage (40), whereas CDI would appear nearly stationary (Fig. 1*C Top*). It follows that a quasi-instantaneous relation for L-type channels can be formed by multiplying instantaneous current–voltage and activation curves, yielding I_L (4*B Right*). Finally, I_L and I_{NL} can be summed to produce the overall quasi-instantaneous current–voltage relation for a cell (I_T) (4*B Right*).

The predictive power of the I_T relation resides in its zero-current crossing points along the voltage axis (ref. 37; Fig. 4*B Right*, open circles). Considering that outward current causes cell hyperpolarization, whereas inward current induces depolarization, we can attribute special features to zero-crossing points, as follows. If the current–voltage relation passes through a crossing point with positive slope (Fig. 4*B Right*, points *r* and *p*), then the cell will tend to reside at this point in a stable fashion. Conversely, if the relation passes with a negative slope (Fig. 4*B Right*, point *t*), then the cell will diverge from this point: slight hyperpolarization from the zero-current point causes further hyperpolarization, and minor depolarization begets further depolarization. With this insight, we can identify point *r* (Fig. 4*B Right*) as the predicted resting potential, with point *t* as the threshold potential, and point *p* as the plateau potential of the action potential. Remarkably, the complex task of understanding the control of APD then reduces to specifying the timing of conditions that eliminate stable point *p* (Fig. 4*B Right*).

This conceptual reduction permits us to conclude in favor of a unique and surprising scenario for the termination of action potentials, although multiple scenarios initially appear plausible. At one extreme (''dominant CDI case''), elimination of point *p* results from time-dependent decay of I_L whereas I_K remains largely stationary (Fig. 4*C Left*). At time t_p during the plateau of the normal action potential (Fig. 4*A*), the sum of time-independent I_{NL} and $I_L(t_p)$ (Fig. 4*C Left*) produces an $I_T(t_p)$ that predicts a well-defined plateau point *p* (Fig. 4*C Right*). By time t_e during the normal action potential (Fig. 4*A*), ongoing L-type channel CDI reduces I_L to the extent shown by $I_L(t_e)$ (Fig. 4*C Left*). Summing a largely unchanged I_{NL} with $I_L(t_e)$ produces an $I_T(t_e)$ (Fig. 4*C Right*), where point *p* has just transformed into a zero-current point *e*, which is unstable by virtue of bracketing outward current segments. From this point on, the instability of point *e* mandates that the action potential inexorably repolarize to the resting potential. Hence, attainment of point *e* signals the end of the plateau phase. At the other extreme (''dominant K activation,'' Fig. 4*D*), attainment of point *e* mainly reflects time-dependent activation of delayed rectifier K currents [$I_{NL}(t_e) \gg I_{NL}(t_p)$], whereas CDI proceeds slowly so that I_L decays little [$I_L(t_e) \sim I_L(t_p)$]. Conventional wisdom has it that the actual scenario resides between these two extremes (12, 14), and all of the scenarios are consistent with properties of the normal action potential (Fig. 4*A*, normal). Now, we come to the important insight: only the dominant CDI scenario in Fig. 4*C* can explain the genesis of ultralong action potentials on elimination of L-type channel CDI. Here, points p' and e' in the ultralong response (Fig. 4*A*), analogs to points *p* and *e* in the normal response, are separated by more than a second ($t_{p'} - t_{e'} > 1$ s), because secondary processes like residual voltage-dependent

inactivation of L-type channels (5) would require such a long time span to produce a decay of I_L commensurate to that in Fig. 4*C*. Alternatively, very slow activation of delayed rectifier K currents, considered insignificant on the time scale of normal responses, may progress sufficiently over a second to contribute to the genesis of point e' and plateau termination. In any of the other scenarios, elimination of CDI would predict only minimal to moderate action-potential prolongation. For example, in Fig. 4*D*, if the time-dependent decrease in I_L (*Left*) were attenuated consequent to the loss of CDI, only slightly greater K channel activation than reflected in $I_{NL}(t_e)$ (*Left*) would be required to produce a plateau-terminating I_T akin to $I_T(t_e)$ (*Right*). Because of the considerable amplitude and rapidity of time-varying K channel activation, little additional time would be required to produce the extra increment of K channel activation, so that action potentials would terminate after only modest prolongation.

The dominant CDI scenario (Fig. 4*C*) thus represents a recast paradigm of action-potential control, one that resolves the paradox raised above as follows. The dominance of L-type channels in controlling APD arises from the faster *kinetics* of CDI compared with ongoing K channel activation during the plateau. By contrast, the *amplitudes* of L-type and K currents must be initially commensurate to generate a stable point *p* (Fig. 4*B*) and thereby an action-potential plateau; the importance of K currents in the genesis of the plateau remains undisputed.

Beyond their implications for normal heart function, our results furnish insight into therapeutic approaches for cardiac arrhythmias in abnormal QT conditions. Novel drugs that promote or disrupt CaM/L-type channel interactions (8, 10) would now present as potent modulators of APD. CaM preassociation and lobe-specificity (Fig. 2) provide enhanced prospects for target selectivity (41) unforeseen in earlier reviews of CaM pharmacology (42). Gene therapy with engineered CaMs offers another approach (43), as CaMs mutated to enhance Ca^{2+} affinity (32) could normalize abnormally long action potentials in long QT disease.

Beyond considerations of cardiac excitability, our experiments bode well for the application of virally delivered, engineered CaMs to probe the biology of other preassociated-CaM signaling pathways. Given the growing number of molecules known to preassociate with CaM (1), we anticipate that this approach will facilitate discovery of the biological impact of related Ca^{2+} feedback loops in diverse tissues.

We thank Dr. Enrico Stefani, University of California, Los Angeles, for suggesting the experiment in Fig. 3*E*. This work was supported by a Specialized Center of Research project of the National Institutes of Health (P50-HL52307 to D.T.Y.).

1. Jurado, L. A., Chockalingam, P. S. & Jarrett, H. W. (1999) *Physiol. Rev.* **79,** 661–682.
2. DeMaria, C. D., Soong, T. W., Alseikhan, B. A., Alvania, R. S. & Yue, D. T. (2001) *Nature* **411,** 484–489.
3. Hoeflich, K. P. & Ikura, M. (2002) *Cell* **108,** 739–742.
4. Dasgupta, M., Honeycutt, T. & Blumenthal, D. K. (1989) *J. Biol. Chem.* **264,** 17156–17163.
5. Imredy, J. P. & Yue, D. T. (1994) *Neuron* **12,** 1301–1318.
6. Zuhlke, R. D. & Reuter, H. (1998) *Proc. Natl. Acad. Sci. USA* **95,** 3287–3294.
7. Xia, X.-M., Falker, B., Rivard, A., Wayman, G., Johnson-Pais, T., Keen, J. E., Ishii, T., Hirschberg, B., Bond, C. T., Lutsenko, S., *et al.* (1998) *Nature* **395,** 503–507.
8. Peterson, B. Z., DeMaria, C. D., Adelman, J. P. & Yue, D. T. (1999) *Neuron* **22,** 549–558.
9. Erickson, M. G., Alseikhan, B. A., Peterson, B. Z. & Yue, D. T. (2001) *Neuron* **31,** 973–985.
10. Zuhlke, R. D., Pitt, G. S., Deisseroth, K., Tsien, R. W. & Reuter, H. (1999) *Nature* **399,** 159–162.
11. Singh, B. B., Liu, X., Tang, J., Zhu, M. X. & Ambudkar, I. S. (2002) *Mol. Cell* **9,** 739–750.
12. Keating, M. T. & Sanguinetti, M. C. (2001) *Cell* **104,** 569–580.
13. O'Rourke, B., Kass, D. A., Tomaselli, G. F., Kaab, S., Tunin, R. & Marban, E. (1999) *Circ. Res.* **84,** 562–570.
14. Marban, E. (2002) *Nature* **415,** 213–218.
15. Colecraft, H. M., Alseikhan, B. A., Takahashi, S. X., Chaudhury, D., Mittman, S., Yegnasubramanian, V., Alvania, R. S., Johns, D. C., Marban, E. & Yue, D. T. (2002) *J. Physiol.* **541,** 435–452.
16. Shubeita, H. E., Martinson, E. A., Van Bilsen, M., Chien, K. R. & Brown, J. H. (1992) *Proc. Natl. Acad. Sci. USA* **89,** 1305–1309.
17. Westfall, M. V., Rust, E. M. & Metzger, J. M. (1997) *Proc. Natl. Acad. Sci. USA* **94,** 5444–5449.
18. Hardy, S., Kitamura, M., Harris-Stansil, T., Dai, Y. & Phipps, M. L. (1997) *J. Virol.* **71,** 1842–1849.
19. Johns, D. C., Marx, R., Mains, R. E., O'Rourke, B. & Marban, E. (1999) *J. Neurosci.* **19,** 1691–1697.
20. Wei, S. K., Colecraft, H. M., DeMaria, C. D., Peterson, B. Z., Zhang, R., Kohout, T. A., Rogers, T. B. & Yue, D. T. (2000) *Circ. Res.* **86,** 175–184.
21. Linz, K. W. & Meyer, R. (2000) *Pflügers Arch.* **439,** 588–599.
22. Keen, J. E., Khawaled, R., Farrens, D. L., Neelands, T., Rivard, A., Bond, C. T., Janowsky, A., Fakler, B., Adelman, J. P. & Maylie, J. (1999) *J. Neurosci.* **19,** 8830–8838.
23. Nerbonne, J. M., Nichols, C. G., Schwarz, T. L. & Escande, D. (2001) *Circ. Res.* **89,** 944–956.
24. Li, G. R., Yang, B., Sun, H. & Baumgarten, C. M. (2000) *Am. J. Physiol.* **279,** H130–H138.
25. Luo, C. H. & Rudy, Y. (1994) *Circ. Res.* **74,** 1071–1096.
26. Marban, E. & Wier, W. G. (1985) *Circ. Res.* **56,** 133–138.
27. Leblanc, N. & Hume, J. R. (1990) *Science* **248,** 372–376.
28. Maltsev, V. A., Sabbah, H. N., Higgins, R. S., Silverman, N., Lesch, M. & Undrovinas, A. I. (1998) *Circulation* **98,** 2545–2552.
29. Deschenes, I., Neyroud, N., DiSilvestre, D., Marban, E., Yue, D. T. & Tomaselli, G. F. (2002) *Circ. Res.* **90,** E49–E57.
30. Tan, H. L., Kupershmidt, S., Zhang, R., Stepanovic, S., Roden, D. M., Wilde, A. A., Anderson, M. E. & Balser, J. R. (2002) *Nature* **415,** 442–447.
31. Balshaw, D. M., Xu, L., Yamaguchi, N., Pasek, D. A. & Meissner, G. (2001) *J. Biol. Chem.* **276,** 20144–20153.
32. Wang, S., George, S. E., Davis, J. P. & Johnson, J. D. (1998) *Biochemistry* **37,** 14539–14544.
33. Mitchell, M. R., Powell, T., Terrar, D. A. & Twist, V. W. (1984) *Br. J. Pharmacol.* **81,** 543–550.
34. Weber, C. R., Piacentino, V., III, Ginsburg, K. S., Houser, S. R. & Bers, D. M. (2002) *Circ. Res.* **90,** 182–189.
35. Bers, D. M. (2002) *Excitation-Contraction Coupling and Cardiac Contractile Force* (Kluwer, Dordrecht, The Netherlands).
36. Matsuoka, S., Nicoll, D. A., Hryshko, L. V., Levitsky, D. O., Weiss, J. N. & Philipson, K. D. (1995) *J. Gen. Physiol.* **105,** 403–420.
37. Noble, D. (1966) *Physiol. Rev.* **46,** 1–46.
38. Noble, D. (1979) *The Initiation of the Heartbeat* (Oxford Univ. Press, Oxford), pp. 64–84.
39. Hille, B. (1992) *Ionic Channels of Excitable Membranes* (Sinauer, Sunderland, MA).
40. Isenberg, G. & Kockner, U. (1982) *Pflügers Arch.* **395,** 30–41.
41. Anderson, M. E. (2002) *J. Cardiovasc. Electrophysiol.* **13,** 195–197.
42. Vincenzi, F. F. (1981) *Cell Calcium* **2,** 387–409.
43. Isner, J. M. (2002) *Nature* **415,** 234–239.